Electrochemical Formation of Pr-Ni Alloys in LiF-CaF2-PrF3 and NaCl-KCl-PrCl3 Melts

AUTHOR(S):

Yasuda, K.; Kondo, K.; Nohira, T.; Hagiwara, R.

CITATION:

Yasuda, K. ...[et al]. Electrochemical Formation of Pr-Ni Alloys in LiF-CaF2-PrF3 and NaCl-KCl-PrCl3 Melts. Journal of the Electrochemical Society 2014, 161(7): D3097-D3104

ISSUE DATE:

2014-02-15

URL:

http://hdl.handle.net/2433/189438

Journal of The Electrochemical Society, **161** (7) D3097-D3104 (2014) D3097
0013-4651/2014/161(7)/D3097/8/$31.00 © The Electrochemical Society

JES Focus Issue on Electrochemical Processing and Materials Tailoring for Advanced Energy Technology

Electrochemical Formation of Pr–Ni Alloys in LiF–CaF_2–PrF_3 and NaCl–KCl–$PrCl_3$ Melts

Kouji Yasuda,[a,b,z] Katsuya Kondo,[a] Toshiyuki Nohira,[a,*,z] and Rika Hagiwara[a,*]

[a]*Graduate School of Energy Science, Kyoto University, Yoshida-honmachi, Sakyo-ku, Kyoto 606-8501, Japan*
[b]*Environment, Safety and Health Organization, Kyoto University, Yoshida-honmachi, Sakyo-ku, Kyoto 606-8501, Japan*

For the establishment of a process for the electrochemical recovery of rare earth elements from used magnet scraps, the electrochemical formation of Pr–Ni alloys in molten LiF–CaF_2–PrF_3 and NaCl–KCl–$PrCl_3$ salts at 1123 K and 973 K, respectively, was investigated. Cyclic voltammetry and open-circuit potentiometry indicated the formation of several phases of Pr–Ni alloys. Alloy samples were prepared by one- or two-step potentiostatic electrolysis using a Ni plate electrode at various potentials. Scanning electron microscopy observations and X-ray diffraction measurements confirmed the formation of $PrNi_2$, $PrNi_3$, Pr_2Ni_7, and $PrNi_5$. The formation potential for each Pr–Ni alloy phase was determined from experimental results. In addition, the optimum electrolysis conditions for the separation of Nd, Dy, and Pr are discussed.

Manuscript submitted February 28, 2014; revised manuscript received April 21, 2014. Published May 14, 2014. *This paper is part of the JES Focus Issue on Electrochemical Processing and Materials Tailoring for Advanced Energy Technology.*

Rare earth (RE) metals have several superior characters such as electric, magnetic, and fluorescence properties and are therefore indispensable as industrial materials throughout the world. Among the many applications of RE metals, the use of neodymium–iron–boron (Nd–Fe–B) magnets—the so-called neodymium permanent magnets—has been remarkably increasing recently. Neodymium permanent magnets composed of a $Nd_2Fe_{14}B$ main phase have several advantages such as superior magnetic properties and high mechanical strength, and are used for voice coil motors in hard disk drives (HDDs), magnetic resonance imaging (MRI), speakers/vibrators in cell phones, and motors in electric vehicles (EVs) and hybrid electric vehicles (HEVs). Since praseodymium (Pr) and Nd have similar chemical properties, they are found in nature in the same ores and their separation is difficult. Thus, in some applications including permanent magnets, a Nd–Pr alloy called didymium (Di) is sometimes utilized. On the other hand, Nd–Fe–B magnets have the drawback of a relatively low Curie temperature of ∼583 K. In order to maintain its superior coercive force even at high temperatures (above 473 K), where high-performance motors in EVs and HEVs operate, dysprosium (Dy) is necessary as an additive.

One of the concerns pertaining to RE magnets is the uneven distribution of RE resources: in 2011, China had 50% of the proven RE reserves and produced over 97% of the global RE supply.[1] In 2010–2012, the price of REs increased sharply, causing supply problems for the magnets. While the present RE production capacity satisfies the demand and their price has lowered, there remains the potential for RE shortage in the future.

On the basis of these supply circumstances, it can be concluded that the recycling or waste management of Nd–Fe–B magnet scraps is currently an urgent task. The conventional wet processes for RE recycling from Nd–Fe–B magnet scraps have several disadvantages such as their multistep and complicated processes, high environmental loads, and large energy consumption. As new recycling methods, pyrometallurgical processes such as chemical vapor transport,[2] selective reduction,[3] molten salt electrolysis,[4] and ionic liquid electrolysis[5] have also been investigated. Nonetheless, a simple, inexpensive, and environmentally friendly recycling process for Nd, Dy, and Pr is desired for utilizing the used magnets that are expected to be discarded from EVs and HEVs in a decade.

We have proposed a new separation and recovery process for RE metals from magnet scraps using molten salts and an alloy diaphragm.[4,6–11] According to our previous studies, a specific RE element can be alloyed and de-alloyed rapidly with iron-group (IG) metals in molten salts by using electrochemical methods.[12] In the proposed process, Nd, Dy, and Pr are separated because of differences in both the formation potentials and formation rates of the RE–IG alloys used as the diaphragm. In order to achieve a high separation factor, the selective formation of RE–IG alloys is required; moreover, it is essential to clarify the formation potential of each RE–IG alloy phase. As the first step in the application of the molten salt electrochemical process to molten halides, the LiF–CaF_2 eutectic melt was selected. We have already reported the formations of Nd–Ni alloys[7,8] and Dy–Ni alloys[9] in molten LiF–CaF_2–REF_3 (0.30 mol%, RE = Nd or Dy) at 1123 K. Concerning the LiF–CaF_2 eutectic melt, Nourry et al. have also reported the formation of Nd–Ni alloys.[13,14] As a second molten halide of choice, we selected the consolute composition of NaCl–KCl (NaCl:KCl = 50.6:49.4 mol%, melting point (m.p.) = 930 K) owing to its high thermal stability and the availability of a stable Ag^+/Ag reference electrode. We have recently reported the formations of Nd–Ni alloys[10] and Dy–Ni alloys[11] in molten NaCl–KCl–$RECl_3$ (0.50 mol%, RE = Nd or Dy) at 973 K.

As the concluding part of a series of fundamental studies on the establishment of our proposed process, the present paper reports on the behavior of Pr that can be a component of Nd–Fe–B magnets. The electrochemical formation of Pr–Ni alloys has been investigated in molten LiF–CaF_2–PrF_3 and NaCl–KCl–$PrCl_3$ salts at 1123 K and 973 K, respectively, with an emphasis on the identification of alloy phases and the clarification of their formation potentials. The optimum electrolysis potential for selective alloy formation in the two molten salts is discussed on the basis of the formation potentials of RE–Ni (RE = Pr, Nd, or Dy) alloys.

Experimental

The details of the experimental setup and procedure have already been reported elsewhere.[8,10] Lithium fluoride (LiF) and CaF_2 were mixed in a eutectic composition (LiF:CaF_2 = 80.5:19.5 mol%, m.p. = 1042 K),[15] and NaCl and KCl were mixed to a consolute composition (NaCl:KCl = 50.6:49.4 mol%, m.p. = 930 K).[16] Two hundred grams of the mixture was loaded into a graphite crucible or a glassy carbon crucible. The experiments were carried out under an Ar atmosphere at 1123 K for the LiF–CaF_2 melt. In the case of the NaCl–KCl melt, the experiments were carried out under an Ar atmosphere in a dried and deoxygenated atmosphere in a glove box at 973 K. Powdery PrF_3 (Kojundo Chemical Laboratory Co., Ltd., 99.9%) or $PrCl_3$ (Kojundo Chemical Laboratory Co., Ltd., 99.9%) was added directly into the melts as a Pr source. A Ni wire, a Mo wire, and a Ni plate were used as the working electrodes. A glassy carbon rod was used as the counter electrode. A Ni wire was adopted as a quasi-reference

*Electrochemistry Society Active Member
[z]E-mail: yasuda.kouji.3v@kyoto-u.ac.jp; nohira@energy.kyoto-u.ac.jp

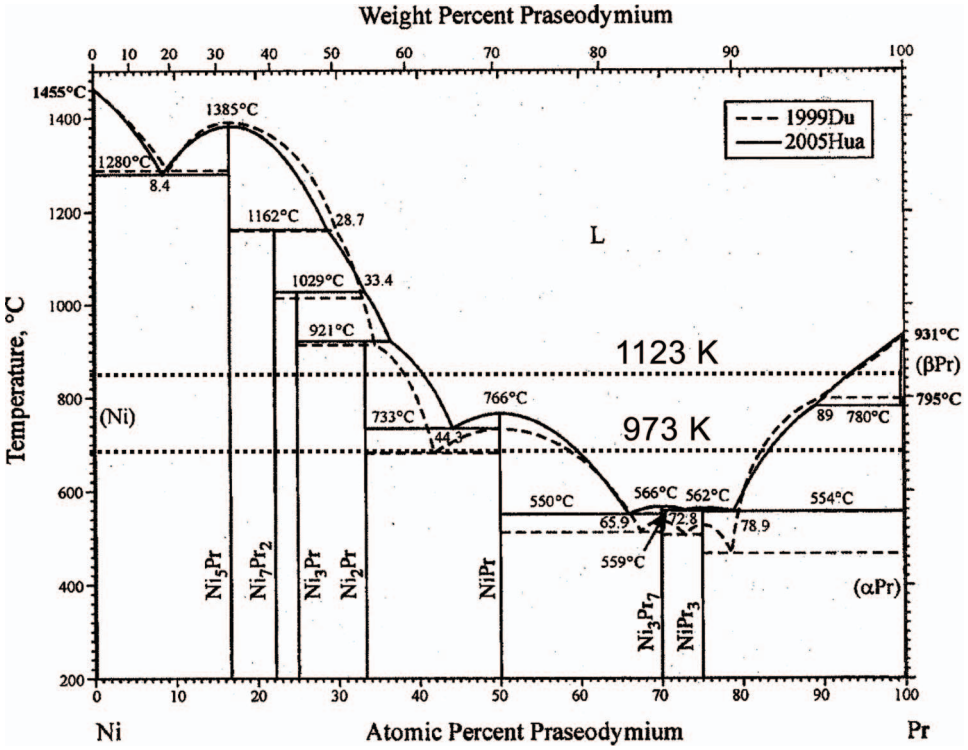

Figure 1. Binary phase diagram for the Pr–Ni system.[17]

electrode in the LiF–CaF_2 melt, and a Ag wire was used as the Ag^+/Ag reference electrode in the NaCl–KCl melt. Potentials were calibrated with reference to Li^+/Li and Na^+/Na potentials in LiF–CaF_2 and NaCl–KCl melts, respectively. All the potentials in this paper are given with reference to the Li^+/Li or Na^+/Na potential. The prepared RE–Ni alloy samples were analyzed by cross-sectional scanning electron microscopy (SEM; Keyence Corp., VE-8800), energy-dispersive X-ray spectroscopy (EDX; Ametek Co., Ltd., EDAX Genesis APEX2), and XRD (Rigaku Corp., Ultima IV, Cu-*Kα*, 0.15418 nm).

Results and Discussion

LiF–CaF_2 system.–Cyclic voltammetry.— The phase diagram of the Pr–Ni system[17] (Fig. 1) shows four intermetallic compounds, namely, $PrNi_2$, $PrNi_3$, Pr_2Ni_7, $PrNi_5$, and a liquid alloy at 1123 K. It is expected that these Pr–Ni alloys are formed electrochemically. In this study, a Mo electrode was occasionally used for comparison with the Ni electrode, because no alloys exist in the binary Mo–Pr, Mo–Li, Mo–Ca, Mo–Na, and Mo–K systems at the present experimental temperatures according to their phase diagrams.[18]

Figure 2 shows a comparison of the cyclic voltammograms for Mo and Ni wire electrodes in a molten LiF–CaF_2–PrF_3 (0.50 mol%) system at 1123 K. For the Mo electrode, only a single pair of redox peaks (B, B′) is observed around 0.2 V (vs. Li^+/Li) except for the redox peaks (A, A′) for Li deposition/dissolution. These peaks correspond to the deposition and dissolution of Pr metal. For the Ni electrode, a cathodic current (C) is observed from approximately 0.6 V, which suggests the formation of Pr–Ni alloys. Several anodic peaks/shoulders (C′) are observed at 0.3 V, 0.4 V, 0.6 V, 0.8 V, and 1.0 V in the anodic sweep, and are possibly caused by the dissolution of Pr from different Pr–Ni alloy phases.

Open-circuit potentiometry.— To determine the deposition potential of Pr metal, the measurement was conducted for a Mo electrode in molten LiF–CaF_2–PrF_3 (0.50 mol%) at 1123 K. By using the same procedures as those employed in our previous studies on Nd and Dy in a LiF–CaF_2 melt,[8,9] the deposition potential of Pr was measured from the transient curve for the open-circuit potential after galvanostatic electrolysis at –3.0 A cm^{-2} for 10 s. The potential stays at 0.21 V for around 120 s, which corresponds to the Pr(III)/Pr potential.

Open-circuit potentiometry is suitable for determining the formation potential of RE–Ni binary alloys.[7–12,19] Thus, open-circuit potentiometry was carried out for the Ni plate electrode after galvanostatic electrolysis at –0.15 A cm^{-2} for 10 min in the same melt. The same measurements were successively repeated thrice to obtain more distinct potential plateaus. Figure 3 shows the three successive open-circuit potentiograms obtained by this process. The potential shifts in the positive direction with time, owing to a decrease in the Pr concentration at the surface of the electrode as Pr atoms diffuse toward the inside of the plate. For the 2nd and 3rd measurements, potential plateaus are observed at 0.33 V, 0.42 V, 0.50 V, 0.82 V, and 1.00 V, which possibly correspond to the equilibrium states of two different Pr–Ni phases, as shown by Eq. 1.

$$Pr_xNi + (y - x)Pr(III) + 3(y - x)\,e^- \rightleftharpoons Pr_yNi \qquad [1]$$

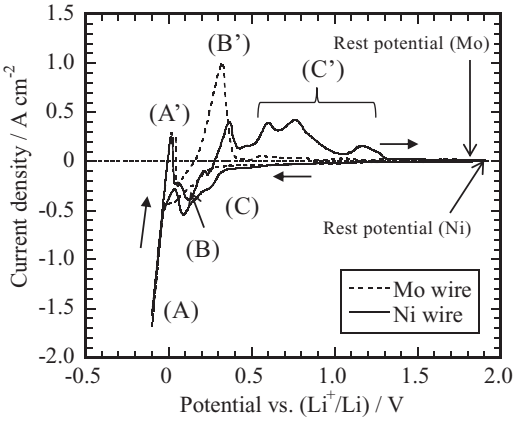

Figure 2. Cyclic voltammograms for Mo and Ni wire electrodes in molten LiF–CaF_2–PrF_3 (0.50 mol%) at 1123 K. Scan rate: 0.05 V s^{-1}.

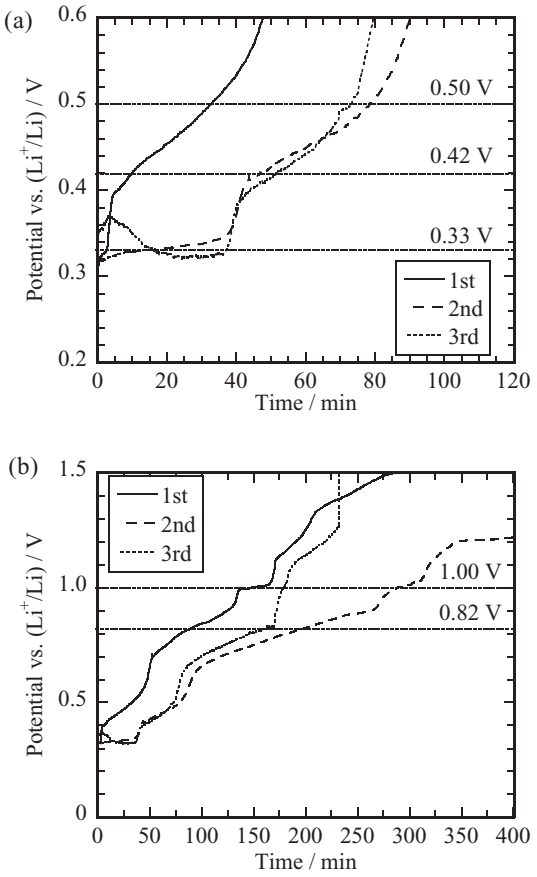

Figure 3. Open-circuit potentiograms for a Ni plate after galvanostatic electrolysis at –0.15 A cm^{-2} for 10 min for 3 cycles in molten LiF–CaF_2–PrF_3 (0.50 mol%) at 1123 K. (a) Initial 120 min, and (b) the whole plots.

Preparation of Pr–Ni alloys and their characterization.— On the basis of the open-circuit potentiometry results, Pr–Ni alloy samples were prepared by the potentiostatic electrolysis using Ni plate electrodes (5 mm × 8 mm × 200 μm) at several potentials. The conditions are summarized in Table I. Sample (F-1) was prepared by the potentiostatic electrolysis using the Ni plate electrode at 0.20 V for 90 min. Figure 4 shows (a) a cross-sectional SEM image of and (b) a powder XRD pattern for sample (F-1). In the SEM image, inhomogeneous alloy formation is observed on both sides of the electrode. EDX analysis revealed the atomic composition to be Pr:Ni = 33:67 at% for the most part of the alloy layer. The Pr concentration is smaller in the vicinity of the Ni substrate, typically 26:74 at% or 18:82 at%. These analytical

Table I. Electrolysis conditions for alloy samples prepared in molten LiF–CaF_2–PrF_3 (0.50 mol%) at 1123 K.

Sample No.	Step	Potential vs. Li^+/Li / V	Time / min
(F-1)	1st step	0.20	90
(F-2)	1st step	0.25	90
	2nd step	0.36	90
(F-3)	1st step	0.25	90
	2nd step	0.60	90
(F-4)	1st step	0.25	60
	2nd step	0.86	60

values suggest a dominant formation of $PrNi_2$ and minor formations of $PrNi_3$ and $PrNi_5$. The powder XRD pattern shown in Fig. 4b confirms that the dominant alloy phase is $PrNi_2$. On the other hand, $PrNi_3$ and $PrNi_5$ were not detected probably owing to their small amounts in the sample. Since the sample and adhered salt was ground together into a powder, the XRD pattern shows the existence of fluoride salts (LiF and CaF_2) and the oxyfluoride of Pr (PrOF). The latter is considered to have formed during the electrolysis from O^{2-} or OH^- impurities in the salt. Here, the pattern for the Ni phase is not observed because it was easily separated from the alloy during the grinding process.

In our previous studies on the electrochemical formation of RE–Ni alloys in molten salts,[7–12,20,21] the following phenomenon was commonly observed. When Ni is used as the working electrode, the formation rates of RE-poor phases such as $RENi_3$ and $RENi_5$ are very slow. On the other hand, once a RE-rich alloy such as $RENi_2$ is formed from the starting electrode, the formation of RE-poor phases, namely, the anodic dissolution of RE metal from the RE-rich alloy, becomes considerably faster. In the present study, therefore, a Pr-rich alloy was formed at 0.25 V (first step) and then a Pr-poor alloy was obtained by the anodic dissolution of Pr (second step).

The analytical results of SEM and XRD for the samples prepared at 0.36 V (sample (F-2)), 0.60 V (sample (F-3)), and 0.86 V (sample (F-4)) for the second step potential are shown in Figs. 5–7, respectively. For sample (F-2) electrolyzed at 0.36 V in the second step, EDX analysis indicated that the dominant and minor compositions in the alloy layer are Pr:Ni = 26:74 at% and 18:82 at%, respectively. The XRD pattern of Fig. 5b clearly agrees with the pattern for the $PrNi_3$ phase calculated by using the PowderCell program[22] from the lattice constant[23] and positional parameters.[24] Thus, $PrNi_3$ is concluded to be the stable phase at 0.36 V. For sample (F-3) prepared at 0.60 V in the second step, EDX analysis showed that the composition for the alloy layer corresponds to Pr:Ni = 18:82 at%. The SEM image in Fig. 6a shows a porous structure for the alloy layer. From the XRD pattern in Fig. 6b, the formation of $PrNi_5$ is confirmed, which indicates that $PrNi_5$ is stable at 0.60 V. When the potential in the second step was set at 0.86 V (sample (F-4)), the SEM image (Fig. 7a) and EDX analysis revealed the formation of porous Ni.

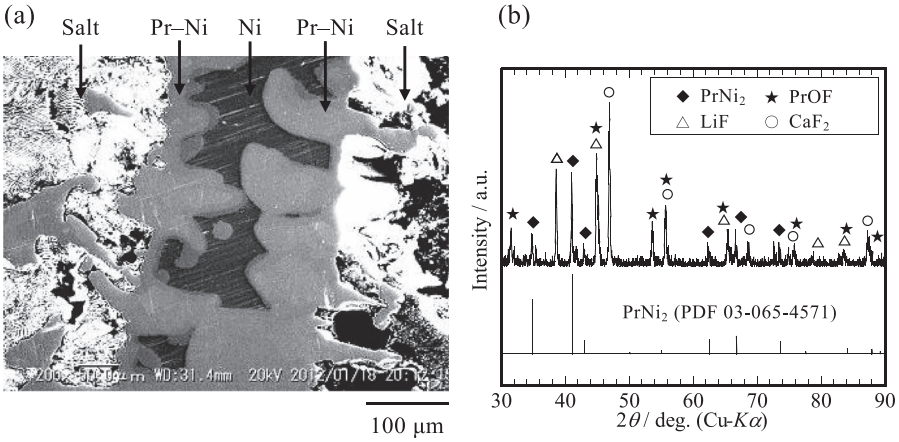

Figure 4. (a) A cross-sectional SEM image of and (b) a powder XRD pattern for sample (F-1) prepared by the potentiostatic electrolysis using a Ni plate electrode at 0.20 V for 90 min in molten LiF–CaF_2–PrF_3 (0.50 mol%) at 1123 K.

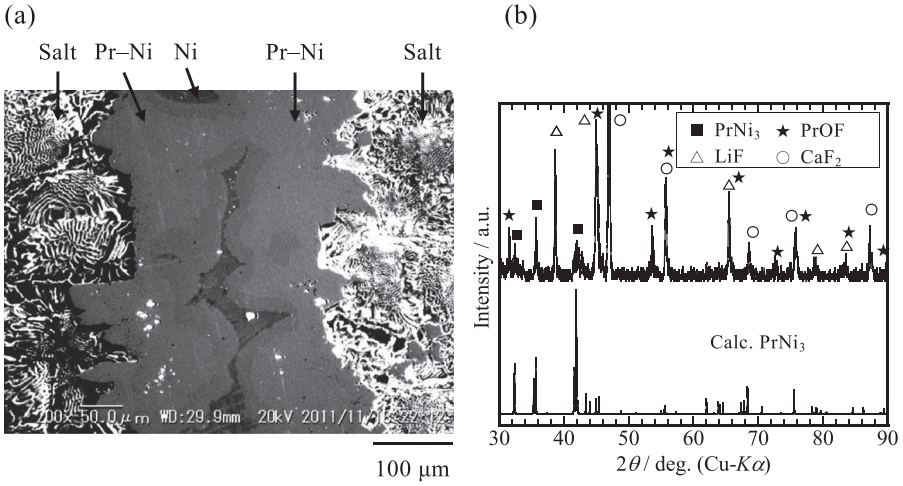

Figure 5. (a) A cross-sectional SEM image of and (b) a powder XRD pattern for sample (F-2) prepared by the potentiostatic electrolysis using a Ni plate electrode at 0.25 V for 90 min and subsequently at 0.36 V for 90 min in molten LiF–CaF_2–PrF_3 (0.50 mol%) at 1123 K.

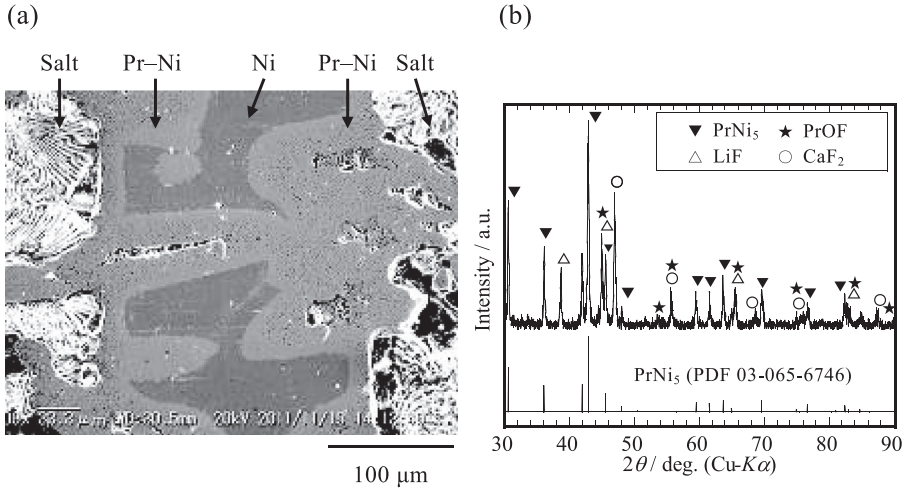

Figure 6. (a) A cross-sectional SEM image of and (b) a powder XRD pattern for sample (F-3) prepared by the potentiostatic electrolysis using a Ni plate electrode at 0.25 V for 90 min and subsequently at 0.60 V for 90 min in molten LiF–CaF_2–PrF_3 (0.50 mol%) at 1123 K.

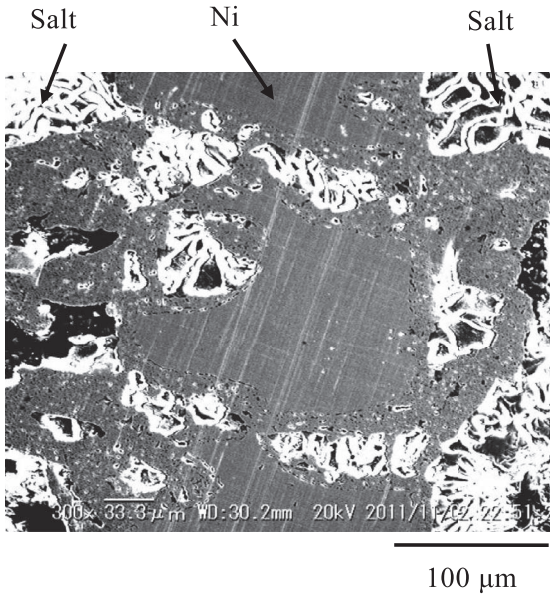

Figure 7. A cross-sectional SEM image of sample (F-4) prepared by the potentiostatic electrolysis using a Ni plate electrode at 0.25 V for 60 min and subsequently at 0.86 V for 60 min in molten LiF–CaF_2–PrF_3 (0.50 mol%) at 1123 K.

Equilibrium potential of Pr–Ni alloys.— From the results, the potential plateau at 0.33 V is ascribed to the following reaction:

$$2\,PrNi_3 + Pr(III) + 3\,e^- \rightleftharpoons 3\,PrNi_2 \quad [2]$$

Considering the number of alloy phases appearing in the binary Pr–Ni phase diagram, the following reaction should exist:

$$3\,Pr_2Ni_7 + Pr(III) + 3\,e^- \rightleftharpoons 7\,PrNi_3 \quad [3]$$

Although the formation of Pr_2Ni_7 could not be confirmed by XRD analysis of samples, the potential plateau at 0.42 V possibly corresponds to the above reaction. If this is the case, since the $PrNi_5$ phase was obtained at 0.60 V, the plateau at 0.50 V would correspond to the reaction given below:

$$\frac{7}{3}PrNi_5 + Pr(III) + 3\,e^- \rightleftharpoons \frac{5}{3}Pr_2Ni_7 \quad [4]$$

The plateau at 0.82 V is attributed to the following reaction:

$$5\,Ni + Pr(III) + 3\,e^- \rightleftharpoons PrNi_5 \quad [5]$$

Finally, the plateau at 1.00 V is possibly derived from the impurities contained in the melt.

Table II lists the formation potentials of Nd–Ni alloys,[8] Dy–Ni alloys,[9] and Pr–Ni alloys in LiF–CaF_2–REF_3 (0.30 mol%; RE = Nd or Dy, 0.50 mol%; RE = Pr) at 1123 K. For the Dy–Ni system, neither a potential plateau nor an XRD pattern was observed for the Dy_2Ni_7 phase.[9] The alloy formation potentials of the Pr–Ni system are almost equal to those of the Nd–Ni system. This result is attributed by the well-known striking similarity in the chemical properties of Nd and Pr. The Nd–Ni and Pr–Ni phases have more negative formation

Table II. Formation reactions and corresponding potentials for RE–Ni alloys and RE metals in molten LiF–CaF_2–REF_3 at 1123 K (RE = Nd, Dy, and Pr). Concentrations of REF_3 are 0.30 mol% for NdF_3 and DyF_3, and 0.50 mol% for PrF_3.

Formation reaction	Potential vs. Li^+/Li / V		
	RE = Nd[8]	RE = Dy[9]	RE = Pr (This study)
$5\,Ni + RE(III) + 3\,e^- \rightleftharpoons RENi_5$	0.73	0.79	0.82
$\frac{7}{3}RENi_5 + RE(III) + 3\,e^- \rightleftharpoons \frac{5}{3}RE_2Ni_7$	0.49	-	(0.50)
$\frac{3}{2}RENi_5 + RE(III) + 3\,e^- \rightleftharpoons \frac{5}{2}RENi_3$	-	0.57	-
$3\,RE_2Ni_7 + RE(III) + 3\,e^- \rightleftharpoons 7\,RENi_3$	0.42	-	(0.42)
$2\,RENi_3 + RE(III) + 3\,e^- \rightleftharpoons 3\,RENi_2$	0.34	0.40	0.33
$RE(III) + 3\,e^- \rightleftharpoons RE$	0.19	0.16	0.21

potentials than the corresponding Dy–Ni phases, while the deposition potential of RE metals shows the opposite trend: Nd(III)/Nd (0.19 V), Dy(III)/Dy (0.16 V), and Pr(III)/Pr (0.21 V).

In a molten LiF–CaF_2 system containing PrF_3, NdF_3, and DyF_3, the effective potential range for the separation of Dy from Pr and Nd is expected to be between 0.34 V and 0.40 V. The thermodynamically stable phases in this potential range are $PrNi_3$, $NdNi_3$, and $DyNi_2$. Further, it is expected that the formation rate of $DyNi_2$ is considerably faster than those of $PrNi_3$ and $NdNi_3$ in this potential range. Thus, it is expected that the formation of $DyNi_2$ would proceed preferentially to that of $PrNi_3$ and $NdNi_3$. Nd and Pr components are expected to remain in the molten salt, and they can be recovered as a Nd–Pr alloy afterward.

NaCl–KCl system.— Cyclic voltammetry.— As shown in Fig. 1, five intermetallic compounds, namely, PrNi, $PrNi_2$, $PrNi_3$, Pr_2Ni_7, $PrNi_5$, and a liquid alloy exist in the Pr–Ni system at 973 K.[17]

Figure 8 shows a comparison of the cyclic voltammograms for Mo and Ni wire electrodes in a molten NaCl–KCl–$PrCl_3$ (0.50 mol%) system at 973 K. For the Mo electrode, only a single pair of redox peaks (D, D′) is observed around 0.2 V (vs. Na^+/Na). These peaks correspond to the deposition and dissolution of Pr metal. On the negative sweep for a Ni electrode, the cathodic currents (E) flow gradually from approximately 0.7 V and increase sharply from 0.4 V, possibly owing to the formation of Pr–Ni alloys. After the reversal of the sweep direction at 0 V, several anodic current peaks appear; this indicates the dissolution of Pr from the different Pr–Ni alloy phases.

Open-circuit potentiometry.— The deposition potential of Pr metal was determined to be 0.23 V by open-circuit potentiometry for a Mo electrode after galvanostatic electrolysis at –0.25 A cm^{-2} for 20 s in molten NaCl–KCl–$PrCl_3$ (0.50 mol%) at 973 K; this procedure is the same as that employed in our previous studies.[10,11]

Subsequently, open-circuit potentiometry was carried out for the Ni plate electrode in order to examine the potentials of Pr–Ni alloy formation. Figure 9 shows the open-circuit potentiogram obtained after galvanostatic electrolysis at –0.03 A cm^{-2} for 3 min. Potential plateaus are observed at 0.38 V, 0.45 V, 0.52 V, and 0.78 V, which correspond to the coexisting states of different Pr–Ni phases. Here, the plateau potentials are determined as the values at which the differential coefficients of the open-circuit potentiogram become the local minima.

Preparation of Pr–Ni alloys and their characterization.— On the basis of the open-circuit potentiometry results, Pr–Ni alloy samples were prepared by the potentiostatic electrolysis using Ni plate electrodes at potentials between the plateaus observed in the open-circuit potentiogram: The conditions are summarized in Table III. A Pr–Ni alloy sample (sample (Cl-1)) was prepared by the potentiostatic electrolysis using a Ni plate electrode at 0.25 V for 40 min. Figure 10 shows (a) a cross-sectional SEM image of and (b) a powder XRD pattern for sample (Cl-1). An alloy layer with a thickness of around 100 μm is observed at both sides of the electrode. EDX analysis revealed

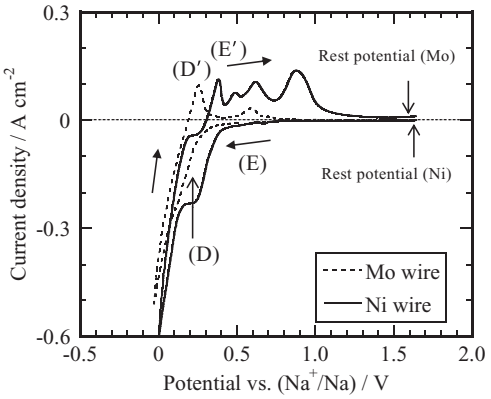

Figure 8. Cyclic voltammograms for Mo and Ni wire electrodes in molten NaCl–KCl–$PrCl_3$ (0.50 mol%) at 973 K. Scan rate: 0.05 V s^{-1}.

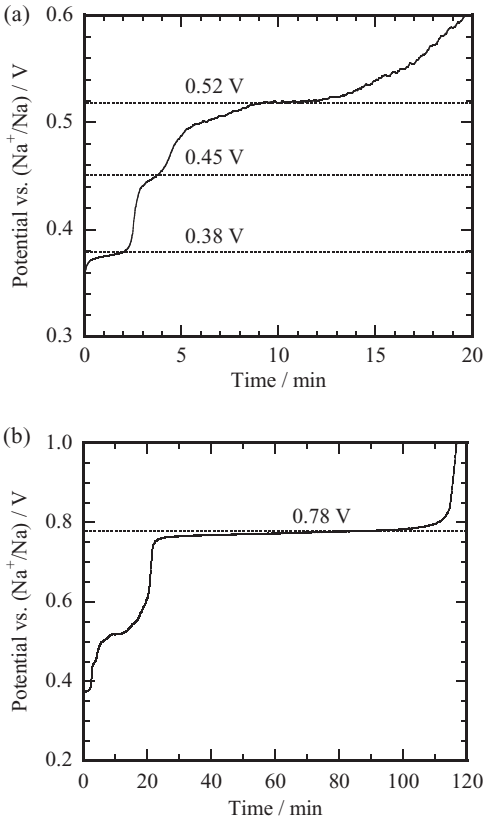

Figure 9. Open-circuit potentiograms for a Ni plate electrode after galvanostatic electrolysis at –0.03 A cm^{-2} for 3 min in molten NaCl–KCl–$PrCl_3$ (0.50 mol%) at 973 K.

Table III. Electrolysis conditions for alloy samples prepared in molten NaCl–KCl–$PrCl_3$ (0.50 mol%) at 973 K.

Sample No.	Step	Potential vs. Na^+/Na / V	Time / min
(Cl-1)	1st step	0.25	40
(Cl-2)	1st step	0.25	42
	2nd step	0.42	40
(Cl-3)	1st step	0.25	40
	2nd step	0.48	50
(Cl-4)	1st step	0.25	40
	2nd step	0.70	55
(Cl-5)	1st step	0.25	40
	2nd step	1.00	60

the atomic composition to be Pr:Ni = 33:67 at% in the alloy layer. The XRD pattern shown in Fig. 10b confirms that the alloy is $PrNi_2$ at the surface of the plate. The formation of PrOCl is also detected. Even at the potential of 0.25 V which was close to the deposition potential of Pr metal (0.23 V), only $PrNi_2$ phase was observed when the electrolysis time was 40 min. According to the phase diagram of Pr–Ni system (Fig. 1), the Pr-richest compound "PrNi" is supposed to be obtained at 973 K. A similar phenomenon had been reported for the formation of Pr–Ni alloys in LiCl–KCl–$PrCl_3$ at 723 K.[21] Only the $PrNi_2$ phase was detected for the sample prepared by the potentiostatic electrolysis using a thick Ni electrode (200 μm) at 0.50 V vs. Li^+/Li for 30 min.[21] Here, the potential was close to the deposition potential of Pr metal (0.47 V). On the other hand, PrNi phase was evidently obtained at 0.50 V by the longer time electrolysis (240 min) using a thin Ni electrode (50 μm).[21] These results were explained by the process that the $PrNi_2$ phase forms preferentially until the whole electrode becomes $PrNi_2$ and the PrNi phase starts to form afterward.[21] Thus, in the present NaCl–KCl system, the PrNi phase would also form by longer time electrolysis at 0.25 V.

Two-step electrolysis was carried out in the NaCl–KCl–$PrCl_3$ melt. In this melt, a Pr-rich alloy was formed at 0.25 V (first step). Figure 11 shows the SEM and XRD results for the samples prepared at 0.42 V in the second step (sample (Cl-2)). A 120-μm-thick alloy layer with the composition Pr:Ni = 26:74 at% is observed. XRD analysis revealed this alloy to be the $PrNi_3$ phase. Thus, the stable phase at 0.42 V is $PrNi_3$.

Figure 12 shows (a) a cross-sectional SEM image of and (b) a powder XRD pattern for sample (Cl-3) that was electrolyzed at 0.48 V in the second step. EDX analysis confirmed that the atomic composition of the surface region was Pr:Ni = 18:82 at%. As shown in Fig. 12b, a distinct Pr_2Ni_7 pattern is observed in the XRD analysis; this observation leads to the conclusion that Pr_2Ni_7 is the thermodynamically stable phase at 0.48 V. For sample (Cl-4) prepared at 0.70 V in the second step, a 100-μm-thick alloy layer is observed in the SEM image (Fig. 13a). According to EDX analysis results, the composition in this layer is Pr:Ni = 18:82 at%. XRD analysis (Fig. 13b) reveals the existence of the $PrNi_5$ phase. Thus, $PrNi_5$ is stable at 0.70 V. When the second electrolysis was carried at 1.00 V (sample (Cl-5)), as shown in Fig. 14, the whole electrode returned to pure Ni. Thus, the Pr–Ni alloy phase is no longer stable at 1.00 V.

Equilibrium potential of Pr–Ni alloys.— On the basis of the above-mentioned results, the formation potentials of Pr–Ni alloys in molten NaCl–KCl–$PrCl_3$ (0.50 mol%) are determined as follows. The potential plateau at 0.38 V in Fig. 9 corresponds to the equilibrium between $PrNi_3$ and $PrNi_2$ (reaction 2). The plateau at 0.45 V is ascribed to the equilibrium reaction between Pr_2Ni_7 and $PrNi_3$ (reaction 3). The potential plateaus at 0.52 V and 0.78 V correspond to the equilibrium reactions of $PrNi_5/Pr_2Ni_7$ and $Ni/PrNi_5$, respectively. The formation potentials of the Pr–Ni alloys and the deposition potential of Pr metal at 973 K are summarized in Table IV. The values for the Nd–Ni and Dy–Ni systems are also listed for reference.

In a molten NaCl–KCl system containing 0.50 mol% of $PrCl_3$, $NdCl_3$, and $DyCl_3$, the effective potential range for the separation of Dy from Pr and Nd is expected to be between 0.39 V and 0.48 V. In this potential range, the thermodynamically stable phases are $PrNi_3$, $NdNi_3$, and $DyNi_2$. Since the formation rate of $DyNi_2$ is considerably faster than those of $PrNi_3$ and $NdNi_3$, it is expected that the formation of $DyNi_2$ would proceed preferentially to those of $NdNi_3$ and $PrNi_3$. As a result, Pr(III) and Nd(III) ions are expected to remain in the molten salt, and they can be recovered as a Nd–Pr alloy afterward.

Comparison of LiF–CaF_2 and NaCl–KCl systems.— Through the experimental results obtained in this study, the formation potentials of Pr–Ni alloys and the effective potential ranges for RE separation in molten LiF–CaF_2 and NaCl–KCl systems have been clarified, as shown in Tables II and IV, respectively. In both these molten salts, the electrochemical behaviors of Nd and Pr were very similar. The separation of Nd and Pr by using the proposed molten salt electrochemical process was found to be difficult. However, this point is not significant because the recovered Nd–Pr alloy (didymium) can be directly used as a raw material for Nd–Fe–B magnets. Since Dy is very scarce and must be distributed at the grain boundaries of magnets, an effective separation ability of Dy from Nd and Pr is important. In this respect, the present molten salt electrochemical process has considerable potential for practical application.

Between LiF–CaF_2 and NaCl–KCl molten salt systems, the former is advantageous from the standpoint of kinetics, as indicated in the voltammograms of Figs. 2 and 8. The formation current for RE–Ni alloys in molten LiF–CaF_2 is higher than that in molten NaCl–KCl, which is probably due to the higher operating temperature for the former. The advantage of NaCl–KCl system is a wider potential region for the effective separation of Dy from Nd and Pr. In addition, its low corrosivity enables a wide selection of cell structure materials. To further optimize the electrolysis condition, the electrode behaviors in

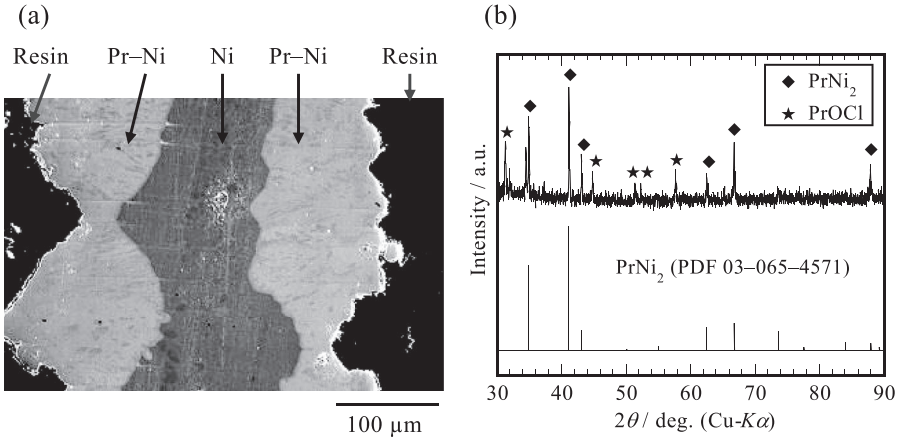

Figure 10. (a) A cross-sectional SEM image of and (b) a powder XRD pattern for sample (Cl-1) prepared by the potentiostatic electrolysis using a Ni plate electrode at 0.25 V for 40 min in molten NaCl–KCl–$PrCl_3$ (0.50 mol%) at 973 K.

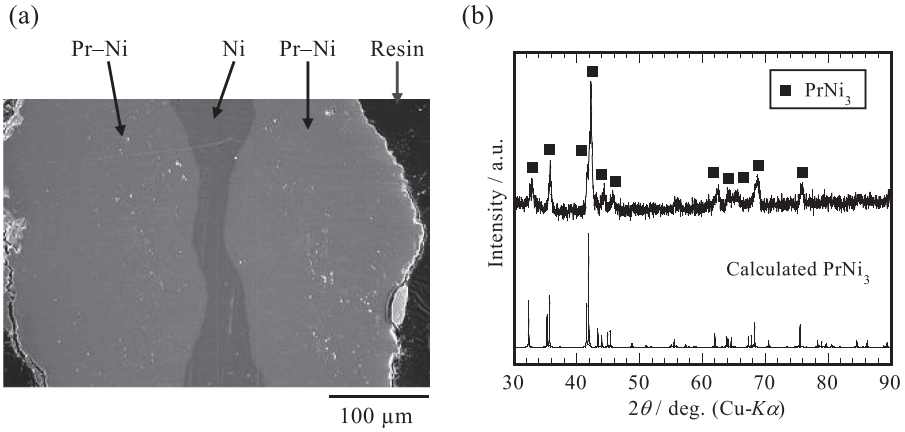

Figure 11. (a) A cross-sectional SEM image of and (b) a powder XRD pattern for sample (Cl-2) prepared by the potentiostatic electrolysis using a Ni plate electrode at 0.25 V for 42 min and subsequently at 0.42 V for 40 min in molten NaCl–KCl–$PrCl_3$ (0.50 mol%) at 973 K.

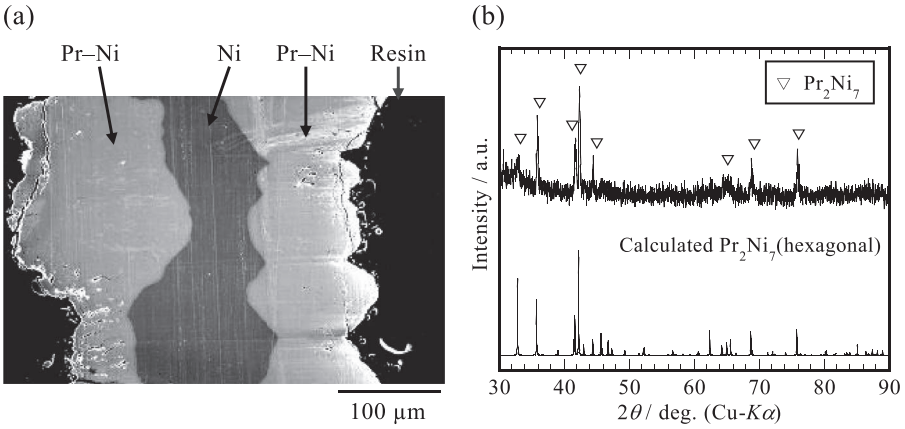

Figure 12. (a) A cross-sectional SEM image of and (b) a powder XRD pattern for sample (Cl-3) prepared by the potentiostatic electrolysis using a Ni plate electrode at 0.25 V for 40 min and subsequently at 0.48 V for 50 min in molten NaCl–KCl–$PrCl_3$ (0.50 mol%) at 973 K.

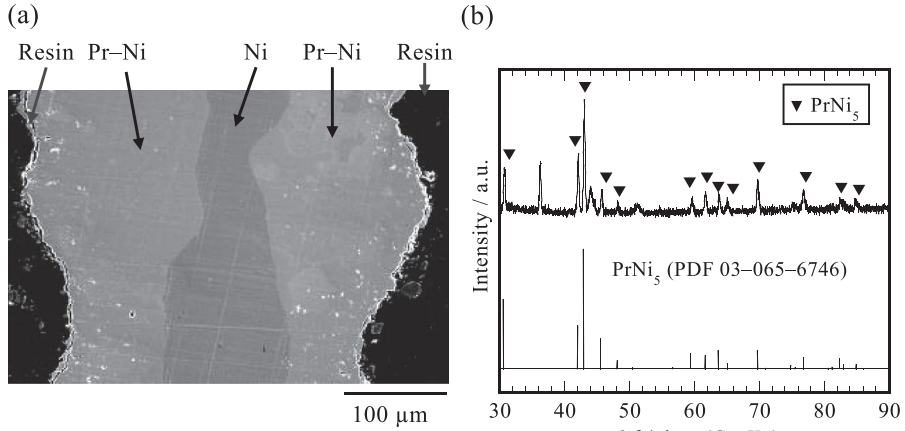

Figure 13. (a) A cross–sectional SEM image of and (b) a powder XRD pattern for sample (Cl-4) prepared by the potentiostatic electrolysis using a Ni plate electrode at 0.25 V for 40 min and subsequently at 0.70 V for 55 min in molten NaCl–KCl–$PrCl_3$ (0.50 mol%) at 973 K.

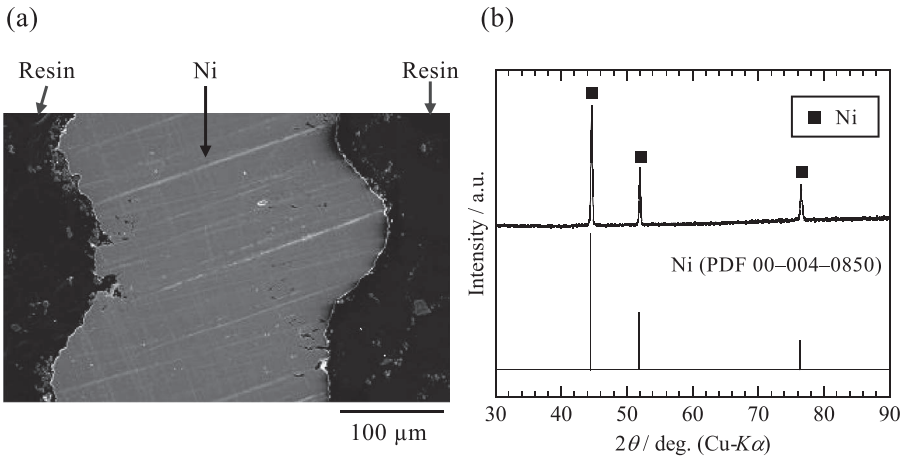

Figure 14. (a) A cross–sectional SEM image of and (b) a powder XRD pattern for sample (Cl-5) prepared by the potentiostatic electrolysis using a Ni plate electrode at 0.25 V for 40 min and subsequently at 1.00 V for 60 min in molten NaCl–KCl–$PrCl_3$ (0.50 mol%) at 973 K.

Table IV. Formation reactions and corresponding potentials for RE–Ni alloys and RE metals in molten NaCl–KCl–$RECl_3$ (0.50 mol%) at 973 K (RE = Nd, Dy, and Pr).

Formation reaction	Potential vs. Na^+/Na / V		
	RE = Nd[10]	RE = Dy[11]	RE = Pr (This study)
$5\,Ni + RE(III) + 3\,e^- \rightleftharpoons RENi_5$	0.79	0.87	0.78
$\frac{7}{3}RENi_5 + RE(III) + 3\,e^- \rightleftharpoons \frac{5}{3}RE_2Ni_7$	0.55	0.72	0.52
$\frac{1}{3}RE_2Ni_7 + RE(III) + 3\,e^- \rightleftharpoons 7\,RENi_3$	0.48	0.64	0.45
$2\,RENi_3 + RE(III) + 3\,e^- \rightleftharpoons 3\,RENi_2$	0.39	0.48	0.38
$RE(III) + 3\,e^- \rightleftharpoons RE$	0.22	0.24	0.23

molten salts containing all the RE halides (RE = Nd, Dy, and Pr) should be investigated on the basis of the information obtained in this study.

Conclusions

The electrochemical formation of Pr–Ni alloys was investigated in molten LiF–CaF_2–PrF_3 (0.50 mol%) system at 1123 K and molten NaCl–KCl–$PrCl_3$ (0.50 mol%) system at 973 K. The results obtained in this study are summarized as follows:

1. The potentials of Dy(III)/Dy were 0.21 V vs. Li^+/Li in the LiF–CaF_2 system and 0.23 V vs. Na^+/Na in the NaCl–KCl system.
2. The open-circuit potentiogram obtained after the galvanostatic electrolysis using a Ni electrode exhibited several potential plateaus corresponding to coexisting states of Pr–Ni phases.
3. The equilibrium reactions of Pr–Ni alloys and the corresponding potentials were determined by SEM/EDX and XRD analyzes of the prepared alloy samples.
4. The effective electrolysis potential ranges for the separation of Dy from Nd and Pr were suggested to be 0.34–0.40 V and 0.39–0.48 V in molten LiF–CaF_2 and NaCl–KCl, respectively.

Acknowledgments

A part of this study was supported by a grant-in-Aid for Scientific Research from the Japanese Ministry of the Environment.

References

1. U. S. Geological Survey, Mineral Commodity Summaries 2012.
2. K. Murase, K. Machida, and G. Adachi, *J. Alloy. Compd.*, **217**, 218 (1995).
3. T. Uda, K. T. Jacob, and M. Hirasawa, *Science*, **289**, 2326 (2000).
4. T. Oishi, H. Konishi, and T. Nohira, Japanese Patent Applications, JPA 2009-287119 (2009).
5. M. Matsumiya, H. Kondo, A. Kurachi, K. Tsunashima, and S. Kodama, *J. Japan Inst. Metals*, **75**, 607 (2011).
6. T. Oishi, H. Konishi, T. Nohira, M. Tanaka, and T. Usui, *Kagaku Kogaku Ronbunshu*, **36**, 299 (2010) (in Japanese).
7. T. Nohira, S. Kobayashi, K. Kobayashi, R. Hagiwara, T. Oishi, and H. Konishi, *ECS Trans.*, **33**, 205 (2010).
8. S. Kobayashi, K. Kobayashi, T. Nohira, R. Hagiwara, T. Oishi, and H. Konishi, *J. Electrochem. Soc.*, **158**, E142 (2011).
9. T. Nohira, S. Kobayashi, K. Kobayashi, K. Yasuda, R. Hagiwara, T. Oishi, and H. Konishi, *J. Electrochem. Soc.*, **159**, E193 (2012).
10. K. Yasuda, S. Kobayashi, T. Nohira, and R. Hagiwara, *Electrochim. Acta*, **92**, 349 (2013).
11. K. Yasuda, S. Kobayashi, T. Nohira, and R. Hagiwara, *Electrochim. Acta*, **106**, 293 (2013).
12. H. Konishi, T. Nohira, and Y. Ito, *J. Electrochem. Soc.*, **148**, C506 (2001).
13. C. Nourry, L. Massot, P. Chamelot, and P. Taxil, *J. New Mater. Electrochem. Syst.*, **10**, 117 (2007).
14. C. Nourry, L. Massot, P. Chamelot, and P. Taxil, *J. Appl. Electrochem.*, **39**, 927 (2009).
15. I. Kostenska, J. Vrbenska, and M. Malinovsky, *Chem. Zvesti*, **28**, 531 (1974).
16. J. M. Sangster and A. D. Pelton, *J. Phys. Chem. Ref. Data*, **16**, 509 (1987).
17. M. Huang and T. A. Lograsso, *J. Alloy. Compd.*, **395**, 75 (2005).
18. T. B. Massalski, *Binary Alloy Phase Diagrams*, ASM International, Materials Park, OH (1996).
19. H. Konishi, T. Nishikiori, T. Nohira, and Y. Ito, *Electrochim. Acta*, **48**, 1403 (2003).
20. T. Iida, T. Nohira, and Y. Ito, *Electrochim. Acta*, **46**, 2537 (2001).
21. T. Nohira, H. Kambara, K. Amezawa, and Y. Ito, *J. Electrochem. Soc.*, **152**, C183 (2005).
22. W. Kraus and G. Nolze, Federal Institute for Materials Research and Testing (BAM), Germany. http://www.ccp14.ac.uk/ccp/web-mirrors/powdcell/a_v/v_1/powder/e_cell.html.
23. A. V. Virkar and A. Raman, *J. Less-Common Metals*, **18**, 59 (1969).
24. D. T. Cromer and C. E. Olsen, *Acta Crystallogr.*, **12**, 689 (1959).